

# Direct phase and amplitude characterization of femtosecond laser pulses undergoing filamentation in air

Johanan Odhner and Robert J. Levis\*

Department of Chemistry and Center for Advanced Photonics Research, Temple University, 1901 N 13th Street, Philadelphia, Pennsylvania 19122, USA

\*Corresponding author: rjlevis@temple.edu

Received February 1, 2012; revised March 14, 2012; accepted March 21, 2012; posted March 21, 2012 (Doc. ID 162427); published May 15, 2012

Measurement of the temporal (spectral) phase and amplitude of a 50 fs laser pulse approaching and exceeding the critical power for self-focusing ( $P_{\text{crit}}$ ) in air reveals the formation of an isolated 17 fs pulse at  $3P_{\text{crit}}$ . The dynamics of self-shortening are measured directly in the filament using transient-grating cross-correlation frequency-resolved optical gating with a noble gas serving as the nonlinear medium. Our results support recent filamentary propagation simulations, suggesting that a Kerr-dominated temporal reshaping process toward the end of the filament is largely responsible for the generation of short pulses. © 2012 Optical Society of America

OCIS codes: 190.7110, 190.3270, 320.2250, 320.7110.

The modification of the temporal and spectral characteristics of a laser pulse undergoing filamentation in the gas phase has been the subject of many experimental and theoretical investigations to date [1,2]. Knowledge of the pulse evolution during filamentary propagation is critical for designing efficient pulse-compression schemes based on filamentation [3], for emerging attosecond technology [4], and for spectroscopic applications [5–8]. Furthermore, accurate measurement of the pulse characteristics as a function of propagation distance and initial power are important for resolving the role of plasma generation in the dynamics of filament formation [9]. While the theoretical understanding of filamentation has advanced rapidly [10], experimental investigations of the dynamic changes in the pulse temporal envelope during filamentation have been limited because the high intensity ( $10^{13}$  Wcm $^{-2}$  [11]) of the pulse in the filament channel results in damage to optical elements in the beam path.

Previous measurements of laser pulses undergoing filamentation have relied largely on extracting a small fraction of the pulse from the filament using a glass plate (either by Fresnel reflection or transmission at grazing incidence) for analysis with frequency-resolved optical gating (FROG) or spectral interferometry [12,13]. Insight into filamentation dynamics has been garnered using these methods, but their application has been limited both by linear and nonlinear effects in the glass inserted into the filament and by material damage, which becomes nonnegligible as filament pulse shortening experiments are scaled to higher (multimillijoule) energies [14,15].

Transient-grating (TG) FROG has been proposed as an alternative geometry suitable for characterizing high-intensity “optical bullets” in a gaseous medium [16]. Here we show that TG cross-correlation FROG (TG-XFROG) largely overcomes the challenges of *in situ* pulse characterization in filaments propagating in a gaseous medium, in this investigation ambient air, at high intensities. We report measurement of the on-axis pulse spectral (temporal) phase and amplitude and focus here on the effects of input power on pulse reshaping at a fixed position in the filament.

In this experiment, a 2.5 mJ, 50 fs pulse (with a transform-limited pulse duration of  $\sim 40$  fs) having an initial beam waist of 4 mm is split into pump and probe pulses. The pump pulse energy and beam diameter is controlled by an iris 5 cm before it is focused by an  $f = 2.07$  m lens into an open-ended tube. The chirp of the input pulse is optimized by using the grating compressor in the amplifier to maximize the spectral blueshift of the pulse in the far field at the highest pump pulse power used in the experiment.

The reference pulse is attenuated using a neutral density filter, passed through a computer-controlled delay stage, and split into two pulses, which are then focused onto the filament in a boxcar geometry (Fig. 1, inset), with a crossing angle of  $\sim 1.1^\circ$ . The spectrograms are processed using commercially available FROG code according to the delay geometry used in the experiment [17]. The beam waist of the reference pulses overlapped in the medium is  $75 \mu\text{m}$ , which defines the spatial aperture used to measure the filament core. Transverse geometric smearing resulting from this small crossing angle can be neglected because of the long duration of the reference pulses, as the smearing is significantly smaller than the length of the measurement. Fine adjustments of the spatial overlap between the filament and the reference pulses are made by optimizing the transverse position

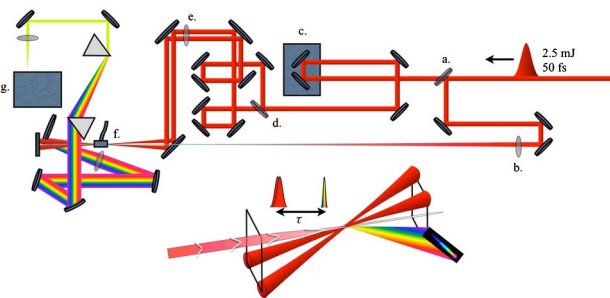


Fig. 1. (Color online) Experimental arrangement for TG-XFROG measurements of a filament. a. 80/20 beam splitter; b.  $f = 2.07$  m lens; c. delay stage; d. 50/50 beam splitter; e.  $f = 0.5$  m lens; f. argon jet; g. USB spectrometer.

of the 2 m lens. Argon gas is introduced into the interaction region between the beams as the nonlinear medium. The direction of time is confirmed by measuring the four-wave mixing signal in air, which shows the effect of the delayed Kerr response on the trailing edge of the gating pulses, as well as revivals due to the rotational wave packets of nitrogen and oxygen generated impulsively by the probe pulses. The diffracted signal exhibits significant spectral angular dispersion resulting from the diffraction of the continuum off of the TG. To avoid directional filtering of the signal [18], the angular dispersion of the signal is corrected by collimating the signal with a lens and recombining the dispersed spectrum using a prism pair. The resulting spatial-chirp-free signal is imaged into a spectrometer (USB4000, Ocean Optics). Spectral recombination could be eliminated by imaging the dispersed spectrum directly onto a CCD camera, allowing for direct detection of the spectrum after the interaction region. Under these conditions, the effective bandwidth of the TG-XFROG is limited mainly by the frequency-dependent efficiency for four-wave mixing [19]. The signal is corrected for this frequency dependence (a squared factor in the power spectrum) and the spectrometer response. Reference pulses are characterized with second-harmonic generation FROG using the same delay stage used in the TG-XFROG measurements, providing an additional check for correct stage alignment.

The spectral phase and amplitude of a pulse undergoing filamentation is characterized using TG-XFROG at a fixed position (255 cm from the 2.07 m lens) as a function of incident laser power. Figure 2 shows the spectrograms measured in the filament channel at different input energies and aperture conditions. The spectrogram representation of a pulse has been suggested as a useful way of visualizing the spectral-temporal dynamics resulting from nonlinear pulse reshaping [20,21], and in this case provides an intuitive representation. The measured XFROG spectrograms were inverted with a standard algorithm and the retrieved temporal and spectral profiles are shown in Fig. 3. The results shown in Fig. 3 emphasize the role of input power on the pulse shaping mechanisms that control the filamentation dynamics. For input powers up to the critical power for self-focusing ( $P_{\text{crit}} = 10 \text{ GW}$  [22]), little spectral or temporal reshaping is observed. As the input power is increased past the critical power for self-focusing, a redshift is observed in the spectrum, indicating the onset of plasma generation. This is immediately followed by temporal pulse splitting, with an accompanying spectral blueshift of the trailing pulse edge (the temporal-spectral dynamics are readily apparent in the spectrograms in Fig. 2). This can be qualitatively understood in the context of recently published numerical simulations that highlight the contributions of plasma-induced breakup (redshifting the leading edge of the pulse) and Kerr-dominated refocusing at the back of the pulse (blueshifting the trailing subpulse) to generate a characteristic double-pulse feature [23]. Only small changes are observed in the pulse spectrum and temporal profile as the power is increased from 20 to 27.5 GW (2 to  $<3$  critical powers, respectively), which we interpret as being due to an insufficient power to initiate a complete second cycle of refocusing in the off-axis pulse

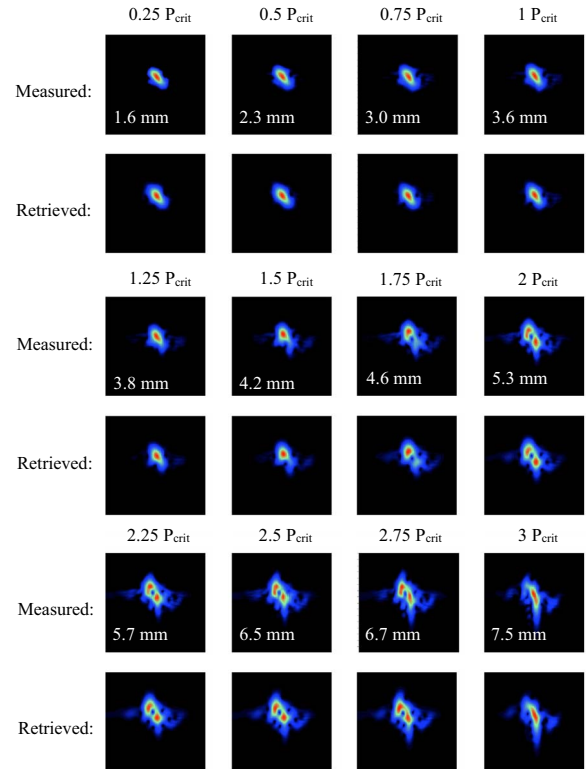


Fig. 2. (Color online) Measured and retrieved spectrograms measured 255 cm from the  $f = 2.07 \text{ m}$  lens at different input powers. The fraction of the critical power and the diameter of the beam aperture are listed for each TG-XFROG trace. The average XFROG retrieval error was 0.0052 and all errors were below 0.0075 on 512 pixel grids.

components that were defocused by plasma generation at the nonlinear focus. However, as the input power is increased to above  $30 \text{ GW}$  ( $3P_{\text{crit}}$ , the trailing pulse becomes the dominant feature of the temporal profile, while the leading pulse is strongly attenuated relative to the trailing pulse, resulting in an overall pulse duration of 17 fs. The fact that an isolated, temporally shortening pulse is observed at  $>3P_{\text{crit}}$  is consistent with previous

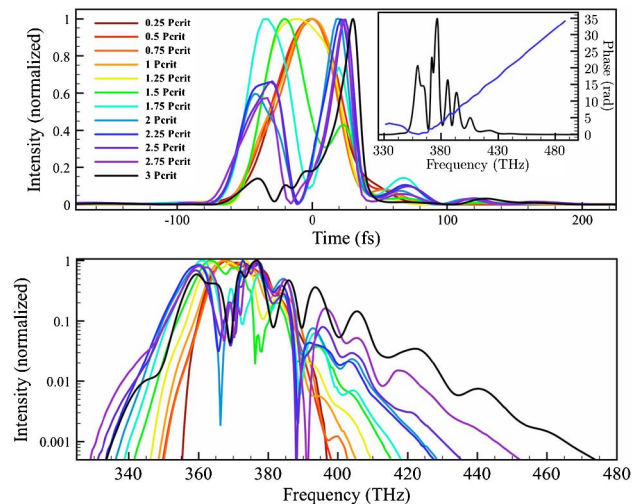


Fig. 3. (Color online) Filament temporal and spectral profiles (normalized intensity) versus longitudinal position in the filament channel measured 255 cm from the 2 m lens. Inset: linear spectrum and phase of the filament pulse at  $3P_{\text{crit}}$ .

experiments and numerical models. Our interpretation of the dynamics is also consistent with our previous measurements under similar conditions [24], where pulse shortening occurred in two stages and where significant pulse shortening in the second focusing event of the filament was inferred from combined spectroscopic and spectral measurements. The observation in [24] of the excitation of water suggests that the pulse duration is further shortened as the pulse power is increased past  $3P_{\text{crit}}$ .

The present measurements span a wide range of input powers and thus provide an importance reference for modeling filament propagation under conditions where plasma generation is expected to play a dominant role in spectral-temporal pulse reshaping. Models of filamentation that consider saturation of the Kerr nonlinearity through higher-order terms as a competitive mechanism for self-focusing arrest predict substantially different filament dynamics than models where Kerr saturation terms are not considered [25]. We expect that modeling the transient pulse structures reported here for different input powers will help shed light on the critical parameters governing pulse shortening during filamentation. The excellent agreement between our measurements and existing theoretical predictions of pulse shortening [14,23] suggest that plasma generation is the dominant defocusing term for filamentary pulse shortening under the conditions reported here. Knowledge of transient pulse structures occurring during filamentation is also essential for nonlinear spectroscopic methods relying on intensity effects and pulse duration effects to generate signals of interest, particularly when multiple-pulse structure can play a role in coherently suppressing or enhancing the nonlinearly generated signal [5,6].

We have demonstrated full characterization of the on-axis temporal envelope of a pulse undergoing filamentation using TG-XFROG. Our results clarify the conditions under which efficient pulse shortening may be realized in a molecular medium (air) for input pulses of the order of 50 fs in duration. The data presented here also suggest that the interplay between Kerr self-focusing and plasma defocusing is adequate for describing the physical process of filamentation. In addition to the insights into filamentation, we have presented a robust method for measuring high-intensity pulses *in situ* that is suitable for measuring pulses of the order of a few optical cycles.

## References

1. A. Couairon and A. Mysyrowicz, Phys. Rep. **441**, 47 (2007).
2. L. Bergé, S. Skupin, R. Nuter, J. Kasparian, and J.-P. Wolf, Rep. Prog. Phys. **70**, 1633 (2007).
3. L. Bergé and S. Skupin, Phys. Rev. Lett. **100**, 113902 (2008).
4. A. Couairon, H. S. Chakraborty, and M. B. Gaarde, Phys. Rev. A **77**, 053814 (2008).
5. J. H. Odhner, D. A. Romanov, and R. J. Levis, Phys. Rev. Lett. **103**, 075005 (2009).
6. F. Calegari, C. Vozzi, M. Negro, S. D. Silvestri, and S. Stagira, J. Mod. Opt. **57**, 967 (2010).
7. J. Kasparian, M. Rodriguez, G. Méjean, J. Yu, E. Salmon, H. Wille, R. Bourayou, S. Frey, Y.-B. André, A. Mysyrowicz, R. Sauerbrey, J.-P. Wolf, and L. Wöste, Science **301**, 61 (2003).
8. H. L. Xu, Y. Kamali, C. Marceau, P. T. Simard, W. Liu, J. Bernhardt, G. Mejean, P. Mathieu, G. Roy, J.-R. Simard, and S. L. Chin, Appl. Phys. Lett. **90**, 101106 (2007).
9. P. Polynkin, M. Kolesik, E. M. Wright, and J. V. Moloney, Phys. Rev. Lett. **106**, 153902 (2011).
10. L. Bergé and S. Skupin, Discrete Contin. Dyn. Syst. **23**, 1099 (2009).
11. H. R. Lange, A. Chiron, J.-F. Ripoche, A. Mysyrowicz, P. Breger, and P. Agostini, Phys. Rev. Lett. **81**, 1611 (1998).
12. A. C. Bernstein, J.-C. Diels, T. S. Luk, T. R. Nelson, A. McPherson, and S. M. Cameron, Opt. Lett. **28**, 2354 (2003).
13. B. Alonso, I. J. Sola, J. S. Román, O. Valera, and L. Roso, J. Opt. Soc. Am. B **28**, 1807 (2011).
14. J. Bethge, G. Steinmeyer, G. S. P. Staudt, C. Brée, A. Demircan, H. Redlin, and S. Dusterer, J. Opt. **13**, 055203 (2011).
15. M. Lenzner, J. Kruger, S. Sartania, Z. Cheng, C. Spielmann, G. Mourou, W. Kautek, and F. Krausz, Phys. Rev. Lett. **80**, 4076 (1998).
16. J. N. Sweetser, D. N. Fittinghoff, and R. Trebino, Opt. Lett. **22**, 519 (1997).
17. D. Lee, P. Gabolde, and R. Trebino, J. Opt. Soc. Am. B **25**, A34 (2008).
18. N. Belabas and D. M. Jonas, J. Opt. Soc. Am. B **22**, 655 (2005).
19. A. Baltuška, M. S. Pshenichnikov, and D. A. Wiersma, in *Frequency-Resolved Optical Gating*, 1st ed., R. Trebino, ed. (McGraw-Hill, 2004), Chap. 14.
20. S. Skupin, G. Stibenz, L. Bergé, F. Lederer, T. Sokollik, M. Schnurer, N. Zhavoronkov, and G. Steinmeyer, Phys. Rev. E **74**, 056604 (2006).
21. S. Akturk, A. Couairon, M. Franco, and A. Mysyrowicz, Opt. Express **16**, 17626 (2008).
22. W. Liu and S. L. Chin, Opt. Express **13**, 5750 (2005).
23. C. Brée, A. Demircan, S. Skupin, L. Bergé, and G. Steinmeyer, Laser Phys. **20**, 1107 (2010).
24. J. H. Odhner, D. A. Romanov, and R. J. Levis, Phys. Rev. Lett. **105**, 125001 (2010).
25. P. Béjot, J. Kasparian, S. Henin, V. Loriot, T. Vieillard, E. Hertz, O. Faucher, B. Lavorel, and J.-P. Wolf, Phys. Rev. Lett. **104**, 103903 (2010).